NASA
Technical
Paper
2166

1983

Rainbow Schlieren

Walton L. Howes
Lewis Research Center
Cleveland, Ohio

National Aeronautics
and Space Administration

**Scientific and Technical
Information Branch**

ERRATA

NASA Technical Paper 2166

RAINBOW SCHLIEREN

Walton L. Howes
May 1983

Page 2, figure 1: The rightmost vertical line should be labeled "Test-section image plane, I."

Pages 7 and 17, equation (3): The symbol θ_f should be θ_{max}.

Page 9, left column, line 11: The word "lean" should be replaced with the word "rich."

Page 11, figure 11: The legend should read "Rainbow schlieren photograph of glycerine settling in water."

Page 11, left column, equation (8) and second line above it: The symbol d_{rms} should be replaced by δ_{rms}.

Page 11, right column, line 4: The symbol d_{rms} should be replaced by δ_{rms}.

Page 12, figure 13: Labels denoting 2a are misplaced.

Page 13, table I, third column: The symbol should be δ_{rms}.

Page 13, table I, fourth column: The symbol should be θ_{rms}.

Page 13, table I, sixth column: The symbols should be $\mu_{rms}/\bar{n}$.

Summary

The rainbow schlieren device was created by replacing the ordinary schlieren knife-edge cutoff with a radial rainbow filter having a transparent center and an opaque surround. This causes most refractive index nonuniformities across the test section to appear varicolored whereas uniformities appear white. The filters were made by photographic size reduction of large radial rainbow transparencies. The large transparencies were produced by revolving sheet color film during exposure to a slit image of a rainbow generated by diffraction of white light.

Rainbow schlieren videotapes and transparencies were recorded of several phenomena involving refractive index nonuniformities. For certain geometries of the nonuniformity it was found possible to quantitatively evaluate refractive index changes by associating image color with light-refraction displacement. The required calculations are simple. In this manner even some turbulence characteristics were evaluated.

The rainbow schlieren displays far more detail of nonuniformities than does an ordinary black-and-white schlieren. For example, thermal waves running across the plate, vortices, and intermittent localized regions of overheated gas could be observed from video recordings of air rising from a hot plate.

Introduction

The schlieren method is one of the oldest, simplest, and least expensive procedures for visualizing nonuniformities in transparent media. Essentially, in the schlieren method light-ray traces deflected from their ideal paths (in the absence of nonuniformities) by refractive index nonuniformities are selectively absorbed to display a variation of irradiance in an image of the nonuniformity. The nonuniformity is thereby revealed.

A schlieren system modified to be a rainbow schlieren is shown schematically in figure 1. (Ordinarily a knife-edge cutoff is located at the position of the rainbow filter.) Light from a point source is collimated by a lens (or mirror), traverses the nonuniformity of interest, is refocused by a decollimating lens (or mirror) to image the light source, and finally is recorded by a camera, which images the nonuniformity. An absorbing filter, usually a knife edge, is introduced at the plane of the light-source image to intercept some of the light refracted by the nonuniformities and hence to produce a nonuniform irradiance of the image of the nonuniformities. The method has been described in greater detail elsewhere (refs. 1 and 2).

In the terminology of Fourier optics the schlieren apparatus Fourier transforms and spatially filters light transmitted by a nonuniform, transparent object and then retransforms the filtered output to recover a spatially filtered image of the object.

The schlieren apparatus has been used as both a qualitative and quantitative device. It qualitatively displays an image of a field of nonuniformities, such as shock waves, whose locations can be measured quantitatively from a schlieren photograph. If the nonuniformities vary slowly spatially, quantitative information regarding the refractive index distribution across the nonuniformity can be estimated if it possesses a simple geometric symmetry (ref. 1), for example, spherical or axial.

Attempts to increase the amount of information extractable from schlieren photography have led to the use of various opaque-filter geometries other than a knife edge as well as transparent, phase-altering filters. The replacement of these neutral density filters by colored filters has added an additional degree of freedom for quantitative interpretation as well as the obvious subjective advantage of color for demonstration purposes.

The variety of filters used for colored schlieren observations is summarized in reference 3. In the present report a new color filter is delineated that provides even more extensive information on spatially extended nonuniformities than the filters described in reference 3.

Principles of Schlieren Method

Geometrical refraction of light serves as the basis of the schlieren method. The theory of light-ray traces is developed in reference 4. In geometrical optics the paths of light rays can be determined by using Fermat's principle. According to this principle, light traces a path for which the transit time between two points is an extremum, usually a minimum (ref. 4, pp. 28f and 86f). The particular path traced by any light ray depends on the refractive index of the medium along the path. If the refractive index is constant along a path in the absence of boundaries, the path is a straight line. Otherwise, the path is curved toward the direction of increasing refractive index, unless the path is already parallel to the refractive index gradient (ref. 5, p. 123). Explicit solutions for the ray traces are very dependent on the geometric symmetry and form of the refractive index function. Several specific solutions for a steady medium are presented in references 4 (e.g., pp. 38 and 164-172) and 6. An additional solution for a randomly inhomogeneous medium is derived in reference 7.

Consider the ideal schlieren apparatus shown in figure 1 with parallel rays incident on the test section T. If the refractive index function in T is constant and equal to that outside T, the light is unrefracted in T and is focused

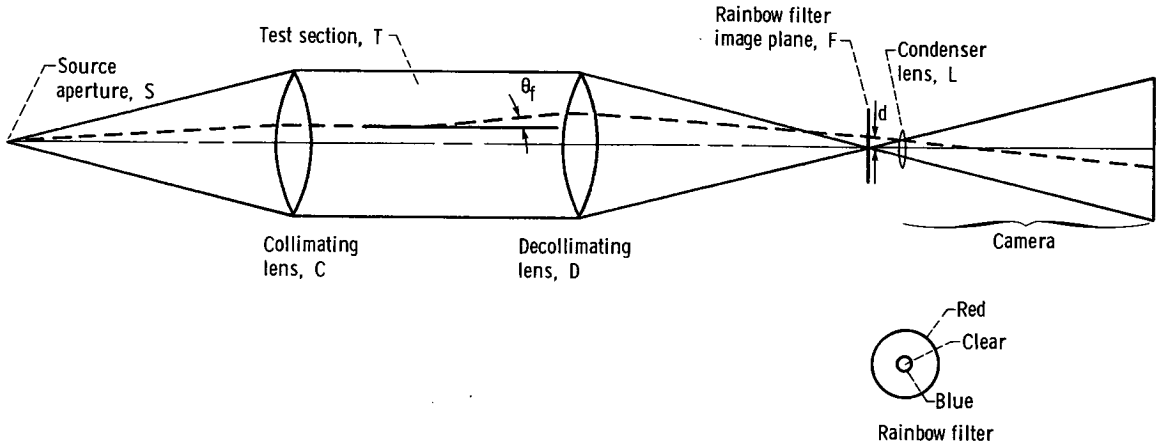

Figure 1. - Rainbow schlieren.

to form a geometric-point image of the light source at F. If the refractive index function in T is not uniform, in general, light will be refracted in T and will be deflected from the geometric-point image of the light source at F. The deflection d at F of ray traces refracted in T is given by

$$d = f \tan \theta_f \tag{1}$$

where f is the focal length of the decollimating lens D, and θ_f is the refraction angle of the ray trace upon emergence from T. (All symbols are defined in appendix A.) Particular refractive index functions can be expressed as implicit functions of θ_f and hence of d. Since d can be measured, it is sometimes possible to evaluate the refractive index (ref. 1). This is worthwhile because in many instances the refractive index is uniquely related to the density, the temperature, or other characteristics of the nonuniform medium. These quantities are important in aerodynamics, heat transfer, and other fields of interest.

Irradiance measurements, as well as deflection measurements, have been used for quantitative analysis of refractive index nonuniformities by the schlieren method (ref. 1). Any real light source is slightly extended, rather than a point. Hence, in the schlieren apparatus the image at F in figure 1 will be slightly extended. A spatial filter consisting of a knife edge at F will therefore produce a gradual, rather than sudden, change of irradiance at the test-section image I as the knife edge is translated across the light-source image. For an ideal apparatus and any given translation of the knife edge the image irradiance at I should be uniform in the absence of nonuniformities in T but will become nonuniform if refractive index nonuniformities exist in T. The nonuniform irradiance reveals the existence and location of the refractive index nonuniformities. Quantitative measurements of the irradiance at I can be related to a reference irradiance distribution associated with known refraction angles, which can, in turn, be related to the refractive index (ref. 1). The irradiance method is sensitive but relatively difficult to apply because a reference irradiance recording is required, and the transmittance of photographic recordings is a variable and nonlinear function of irradiance.

Deflection measurements can be made by replacing the knife edge with a grid at F in figure 1 (ref. 1). Assume that a linear grid is positioned so that undeflected light that forms the image of the light source at F passes between the opaque bars of the grid and is therefore transmitted to the test-section image I. Light refracted by nonuniformities in T may also be transmitted to I through the grid or else may be intercepted by opaque bars of the grid. The resulting image at I appears similar to an interferogram except that lines of uniform intensity represent lines of constant deflection associated with a component of the refractive index gradient rather than lines of constant optical-path difference. The deflection method is relatively insensitive because the grid lines must be sufficiently widely spaced to minimize diffraction effects. Otherwise, accuracy is reduced because of a consequent loss of image resolution when light passes through a narrow slit.

To evaluate a refractive index distribution, two refraction measurements are important, namely the deflection d of the light and the direction of the deflection. For an amplitude filter the image displays the component of deflection perpendicular to lines of constant transmittance by the filter. For example, a knife edge and a linear grid will provide information regarding the direction and magnitude of a component of deflection perpendicular to the knife edge or grid lines. In the absence of irradiance measurements the knife edge provides information on the sense of a component of the deflection but not its magnitude (unless the nonuniformity is stationary in time so that the knife edge can be advanced stepwise between measurements). On the other hand, the grid indicates a deflection component

but not its sense. However, the grid does provide information on the magnitude of the refraction component, but only if the deflection is a monotonic function of the spatial coordinates. This limitation arises because, in a given direction, nonmonotonic deflection due to refraction cannot be distinguished unless the grid rulings are somehow individually labeled.

If the filter transmittance varies radially and the aperture of the light source is circular, the limitations on determining the magnitude of deflections are the same as for the linear filter. However, with regard to direction, lines of uniform irradiance in the image now have a more general significance in that they correspond to lines of constant total deflection rather than to only one component of the deflection. For certain symmetries of the refractive index field the lines of uniform irradiance possess even greater significance. Specifically, for light incident normally (1) to a one-dimensional refractive index gradient contained within a fixed span or (2) to the axis of an axially symmetric refractive index field having constant diameter, the lines of uniform irradiance correspond to lines of uniform refractive index or whatever else can be uniquely related to the refractive index in the particular circumstance. This generality, of course, also applies to a medium with symmetry about a point.

In attempts to gain further information from the schlieren technique, colored filters have been introduced.

Color Filtering

Although the introduction of a colored spatial filter at the light-source-image plane greatly improves the subjective appearance of the schlieren image, additional objective technical benefits may also accrue (ref. 3). With regard to the specific questions of deflection and direction, it appears that the principal benefit of color is in labeling the refraction with respect to direction and magnitude. For example, bicolor and tricolor linear filters have been used (ref. 3) to determine the direction of a component of refraction, as does the knife edge. By extending this concept a filter consisting of different-colored quadrants has been used (ref. 3) to better resolve the direction of refraction. This benefit of color is beyond the capability of existing methods of neutral density filtering with a single photographic exposure.

As stated previously, the circular grid is inadequate for measuring ray-trace deflections if the deflection is a nonmonotonic spatial function because individual grid lines are not identifiable in the image of the nonuniformity. This is usually the case. However, a filter consisting of concentric annuli of different colors should overcome this limitation because each color is identifiable in the image of the nonuniformity. To accomplish this, a new filter was devised that, when introduced in an ordinary schlieren apparatus, provided a system that will be called a rainbow schlieren.

Rainbow Filter

If concentric, annular, colored filters are used in a schlieren apparatus, each color can be associated with a specific range of refraction displacements. By using a continuous, rather than discrete, color change the potential number of colors and hence the resolution of measured displacements is increased. Also, diffracting boundaries between colors should be eliminated. An obvious source of continuous change of color is the spectrum of white light, as in a rainbow. Radial rainbow filters were manufactured by using the simple apparatus shown in figure 2. In the apparatus, light from a zirconium concentrated-arc lamp (Sylvania C10P-DC, 10 W) is focused on a small circular aperture A and then subsequently collimated by lens C. The collimated light passes through a narrow slit S and is then diffracted by a linear grating G with the grid lines perpendicular to the slit length. Since the light is "white," a linear rainbow spectrum appears in the two first-order, diffracted beams. A large achromatic camera lens C_1, is introduced in one of the diffracted beams to collect and focus the diffracted light of all colors. A second, camera lens C_2 is inserted to reduce the spectrum to the desired length for recording in the image plane I. Since collimated monochromatic beams emerge from the grating and are focused at image plane I, the lens combination C_1 and C_2 is effectively focused at infinity. To convert the linear spectrum at I into a radial spectrum, the photographic, color-recording medium is mounted on a motor-driven, rotating disk with the axis of rotation X parallel to the optical axis. The axis of rotation is laterally displaced from the optical axis so that one end of the visible spectrum, either violet or red, is adjacent to the axis of rotation. Then, if the photographic exposure is much greater than the period of rotation of the image plane, a radial rainbow transparency is easily recorded.

To permit accurate adjustment of the recording system, large radial rainbows, 58 mm in diameter, were recorded on 4- by 5-in Kodak Daylight Ektachrome (ASA 64) film. Transparencies were recorded either with a blue center or a red center.

The transparencies recorded by using the apparatus shown in figure 2 were much too large to be used as schlieren filters since the refraction displacements to be measured were at most only a few millimeters. Thus to properly size the filters, the apparatus shown in figure 3 was used. A small, rotating ground glass G and a large scatter-plate diffuser S were inserted between a high-pressure, xenon short-arc source L (Pek Labs X-75, 75 W) and a lens C in order to diffuse light transmitted through the large rainbow transparency I. The scatter

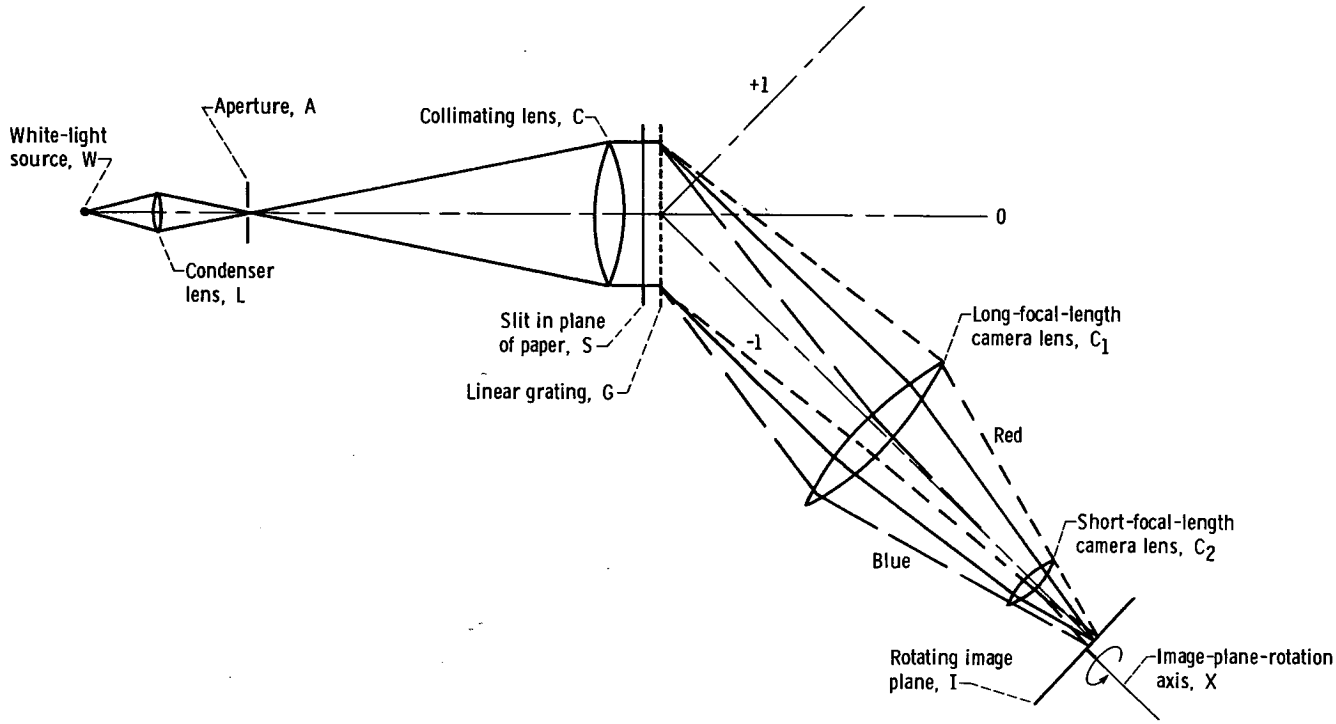

Figure 2. - Arrangement for making radial rainbow transparencies. Order of diffraction, -1.

plate S was separated as much as possible from the transparency I in order to minimize transmission of scatter-plate granularity to the final filter image at F.

Because it was inconvenient to move a large diffuser during the photographic exposure, it was hoped that the preceding configuration would be satisfactory. Unfortunately, it was not. The filter copies were granular.

With the aperture A (fig. 3) removed, a demagnified image of the rainbow transparency was recorded at object distances of 127 to 305 cm by a remote 35-mm camera represented by the lens C_a and image plane F. This procedure yielded a filter with a colored center that provided very colorful schlieren images. However, from the technical standpoint a filter with a colored center is inefficient because the central color is wasted in displaying regions where conditions are uniform. Thus, before copying the entire color transparency, the aperture A was inserted in the beam to block all except the center of the transparency. A long overexposure was made to produce a transparent center in the final filter. Then, the aperture A was removed and the transparency was normally exposed to record the colored filter. The transparent center should be large enough to pass the image of the light source in the absence of nonuniformities, and the filter should be just large enough to pass all light deflected by nonuniformities under study. To achieve the maximum deflection resolution, the light source should be as small as possible

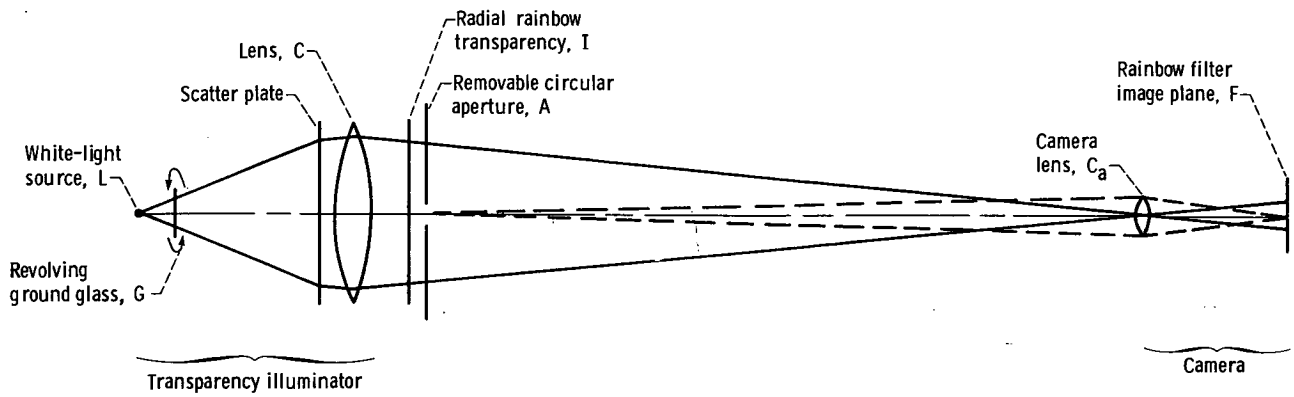

Figure 3. - Arrangement for making rainbow filters.

so that its image is as small as possible, but not so small as to produce a significant diffraction image of the light source. The potential problem of centering the aperture A in the center of the filter was ameliorated by the fact that the end of the spectrum did not precisely coincide with the center of the filter. This left a central dot on the filter, which made it easier to center the aperture A.

The proper combination of filter and transparent-center diameters was actually determined empirically by making a large number of filters of various sizes and then trying them out in experiments. Filters were made with blue centers, red centers, and clear centers with blue or red peripheries, all against an opaque surround. More specific characteristics of these filters are discussed in succeeding sections. An enlargement of a typical filter is shown in figure 4.

Schlieren Apparatus

The schlieren apparatus used to test rainbow filters was a conventional, single-pass system, as shown in figure 1. The light source was a high-pressure, xenon, short-arc lamp (Pek Labs X-75, 75 W) operated continuously. The lamp housing included a condenser lens (not shown in fig. 1) to provide an image, at S, of the source. A small aperture sufficiently large to permit color photography of moderately moving fluid flows was located at this image, which represented the effective source for the schlieren system. The components of the schlieren apparatus had the following dimensions:

(1) Source aperture S: 37 μm

(2) Collimator C and decollimator D: 12.7-cm-diameter, 62.87-cm-focal-length, achromatic lenses

Various cameras were used. First, a videotape system was used to obtain quickly recoverable records for comparing results with different filters. The tapes were also useful for illustrating moderate-speed, dynamic effects in nonuniform flows. After the best filter was selected for a given experiment, rainbow schlieren transparencies of various refractive index nonuniformities were made by using 35-mm Kodak Daylight Ektachrome film with ASA speeds of 64, 400, or 800 (ASA 400 film exposed and developed to obtain ASA 800) depending on the requirements for sufficient exposure and for stopping flow movements. Finally, a semitransparent, Mylar pellicle inclined at 45° to the optical axis was introduced ahead of the filter plane F to obtain two light-source-image points and two separate, simultaneous, schlieren recordings: one, the reflected image, in color by using a rainbow filter, and the other in black and white by using a knife edge. This setup permitted comparison of the rainbow schlieren imagery with ordinary black-and-white schlieren imagery. Because of the coarseness of the pellicle as a transmitting medium the reflected beam was used to obtain the best possible color imagery.

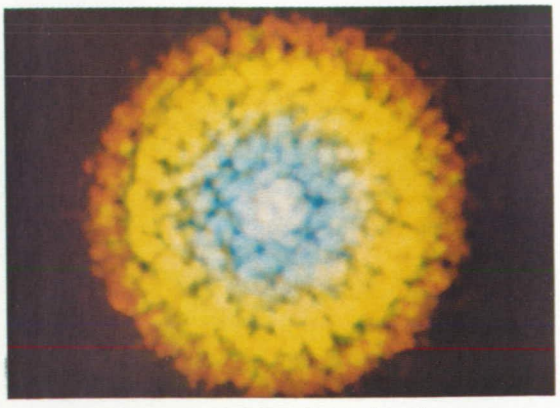

Figure 4. - Rainbow filter (enlarged).

The following cameras were used:

(1) Color videotape: Sony Model DXC-1610 camera with lens replaced by 85- to 250-mm focal length, f/5 autozoom Zuiko lens

(2) Color transparencies: Olympus OM-2N camera with 85- to 250-mm focal length, f/5 autozoom Zuiko lens

(3) Black-and-white film: Nikon F with 135-mm focal length, f/3.5 telephoto lens

In the schlieren apparatus the image size is chosen to correspond to the film size. The image distance in the camera is determined by the beam divergence angle, which, in turn, is defined by the f/number of the decollimating lens D in figure 1. Since the camera must be focused on the object plane T, which is usually remote from the decollimator D, the object and image distances are likely to be large, thus necessitating the use of a long-focal-length camera lens, as exemplified by a telephoto lens.

In making simultaneous exposures in color and black and white it would have been desirable to have a twin cable release to actuate the two shutters. Since the cameras were made by different manufacturers and had different shutter release mechanisms, this was not convenient. Rather, the two shutters were separately actuated manually at times that probably differed by less than 0.1 sec. In general, this time difference did not seriously affect the comparison between the two photographs.

Both still cameras had automatic exposure mechanisms, so that the exposures were not tabulated. However, in nearly all instances the exposures were less than 0.01 sec and in some cases as short as 0.001 sec.

Applications

The rainbow schlieren was demonstrated in a variety of simple applications to test its potential usefulness. The

applications included

(1) Acetylene torch
(2) Oxyacetylene torch
(3) Candle
(4) Match
(5) Hot plate
(6) Horizontal aluminum plate suspended above hot plate
(7) Glycerine mixing with water
(8) Plastic sheet
(9) Low-subsonic, heated-air blower
(10) Cold-air jet
(11) Interaction of cold-air jet with warm-air jet
(12) Bubble
(13) Nonlinear crystal with imposed high voltage
(14) Hand
(15) Breath

Color videotape recordings were made of all demonstrations. Rainbow schlieren transparencies were recorded of those demonstrations that produced the best color effects. Ordinary black-and-white schlieren photographs of most of these objects (items (1) to (8)) were made for comparison with the rainbow schlieren results.

The largest refraction displacements were obtained in those situations involving relatively large variations of refractive index or large extent, or variations in extent, of the refractive index nonuniformity in the direction of the optical axis. These conditions prevailed for items (1) to (8). For items (9) to (15) the aforementioned conditions were not sufficient to produce good refraction color effects with the facilities available. Rather, diffraction color effects were observed in these tests.

Some observations associated with specific tests are discussed in the following sections:

Flames (Items (1) to (4))

Flames produced vivid color effects as shown, for example, in figure 5(a), which displays the refraction field caused by an acetylene torch with a nozzle-exit diameter of 4 mm. (The temperature field could be calculated from the refraction field.) This rainbow schlieren photograph was obtained by using a radial rainbow filter 1.06 mm in diameter with a clear center 0.11 mm in diameter surrounded by blue and ranging out to red at the periphery, all in a black surround. These filters were found to produce better results than those with red innermost.

Unlike the candle and match flames (items (3) and (4)), which were easily disturbed by stray air currents in the laboratory, the acetylene flames were very steady because of the high dynamic pressure of the combustible gases relative to that of ambient disturbances. The refraction field shown in figure 5(a) possesses good axial symmetry despite the tilt of the nozzle from vertical ($\approx 3.7°$) and enough (11) detectable color variations to permit quantitative evaluation of the refractive index. It is evident from the sequence of colors that, proceeding from the outer boundary inward toward the flame axis, the refraction displacement increases until the red isochrome (line of constant color) is reached and then decreases to zero as the axis is approached. The asymmetry of the rainbow colors in the radial direction about the red isochrome results more from the large

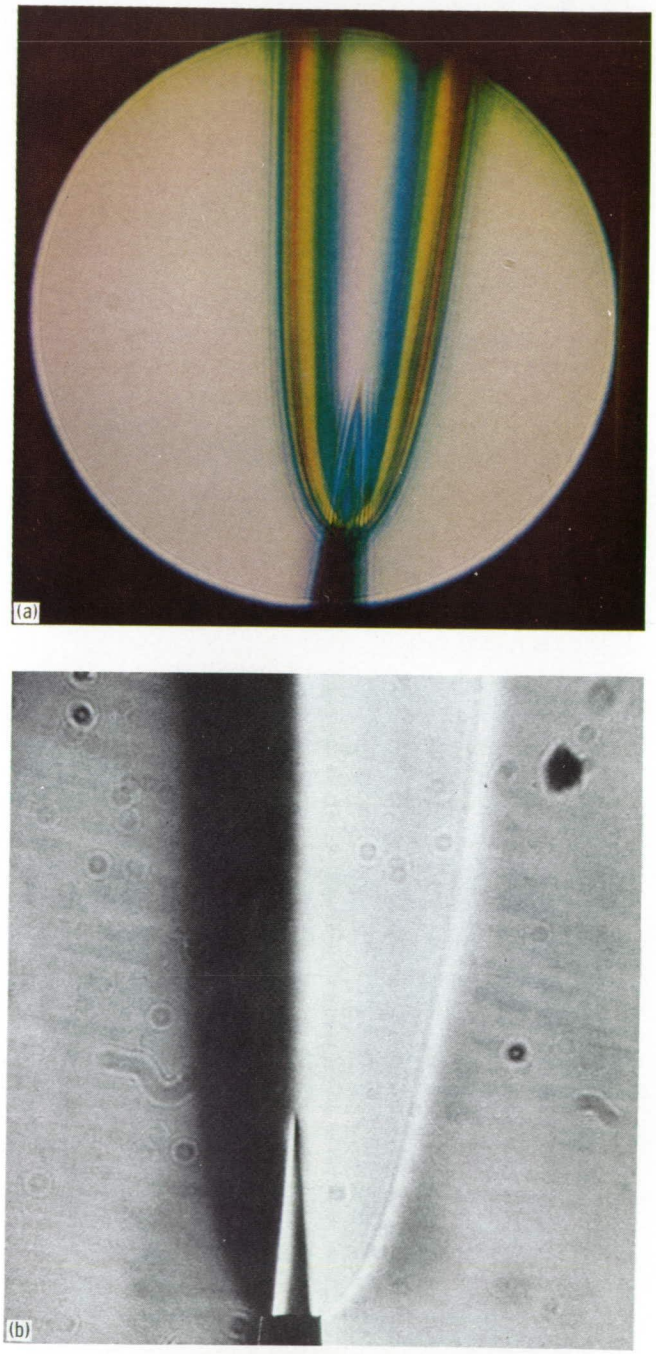

(a) Rainbow schlieren.
(b) Black-and-white schlieren.

Figure 5. - Schlieren photographs of acetylene torch.

variation of light path through the temperature field as a function of radius than from asymmetry of the temperature profile. The conical region with its base at the nozzle-exit plane outlines the core of the jet of combustible gas. The flame itself was bright orange-yellow because of low pressure in the tank of acetylene gas. However, no evidence of this self-illumination appears in the photograph.

The tremendous increase in the amount of information provided by the rainbow schlieren becomes evident by comparing figure 5(a) with figure 5(b), which shows an ordinary black-and-white schlieren photograph of the acetylene flame obtained by using a knife edge oriented parallel to the flame axis. From figure 5(b) the direction of the refraction component normal to the flame axis can be determined, but not its magnitude.

The biggest defect in the schlieren photographs, both color and black and white, is diffraction fringes. These fringes are discussed in the section entitled "Diffraction."

Figure 6 shows a color schlieren photograph of the acetylene torch operating at a gas pressure reduced from that used when recording figure 5. In the condition shown the flame is clearly unstable, as evidenced by the periodic fluctuation of the breadth of the temperature field. The automatic exposure—greater than 1 msec in recording figure 6—appears to have been sufficient to "freeze" the motion of the temperature field except at the "waist" of the boundary oscillation, where the diffraction fringes are blurred.

The axial symmetry of the acetylene flame in figure 5(a) is sufficient to permit evaluation of the refractive index distribution in that part of the heated region where refraction occurs. The maximum refraction displacement d_{max} in this example is less than the radius, 0.53 mm, of the rainbow filter. Hence, by virtue of equation (1) the maximum refraction angle θ_{max} is less than $\tan^{-1}(d_{max}/f) = \tan^{-1}(0.53/629) = 8.4\times10^{-4}$ rad $= 0.048°$, so that θ_f is small.

Equations for evaluating continuous, spherical, refractive index distributions $n(r)$ when θ_f is small are derived in appendix B from figure 7, which shows details of a ray trace in a medium for which the radius–refractive index product $n(r)r$ is monotonic. The resulting formulas also apply for a cylindrical refractive index distribution $n(r)$ with $r=(x^2+y^2)^{1/2}$ if the light is initially parallel to the x axis, as in the present instance.

In appendix B the refractive index n is evaluated in the form of the relative difference $(n_m-n_0)/n_0$, where n_m is the refractive index at radius r_m and n_0 is the ambient value. More specifically, $(n_m-n_0)/n_0$ is associated with a light-ray trace initially incident on the distribution $n(r)$ at the ordinate value y_0. This ray trace achieves a minimum radius r_m and from the schlieren image appears to originate at an object point having the ordinate value y_P. Thus, y_P can be determined from the schlieren image, but y_0 and r_m must be determined by some other means, namely by calculation from other measurable quantities. For small values of θ_f, as in the present experiment, the difference among y_P, y_0, and r_m is negligible, so no detailed calculations are required. Specifically, according to inequality (2) in appendix B, with the camera focused on the object plane containing the axis of symmetry, that is, $r=0$, of the field $n(r)$ the values of y_P and r_m differ by

$$|y_P-r_m| < \left|\frac{r_0\theta_{max}}{4}\right| \tag{2}$$

where r_0 is the outermost radius at which $n(r)$ approaches the constant ambient value n_0. In the present instance $r_0<9$ mm, as determined from the rainbow schlieren image (including its magnification), so that $|y_P-r_m|<2\times10^{-3}$ mm, which is within the error of the distance measurements. Next, the distortion Δ, that is, the separation of the apparent and real object points, y_P and y_0, respectively, is given by

$$\Delta \equiv y_P-y_0 < \frac{r_0\theta_f^2}{2} \tag{3}$$

according to inequality (3) in appendix B. Because of its proportionality to θ_f^2, Δ is certainly negligible. Specifically, $\Delta<4\times10^{-6}$ mm. From the foregoing results, $y_P\approx y_0\approx r_m$, so that only $(n_m-n_0)/n_0$ need be evaluated. As shown in appendix B,

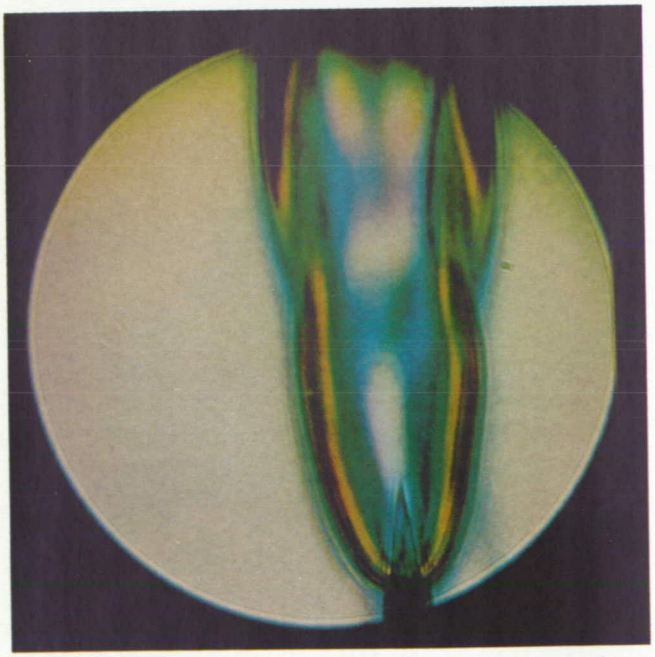

Figure 6. - Rainbow schlieren photograph of acetylene torch operating unstably.

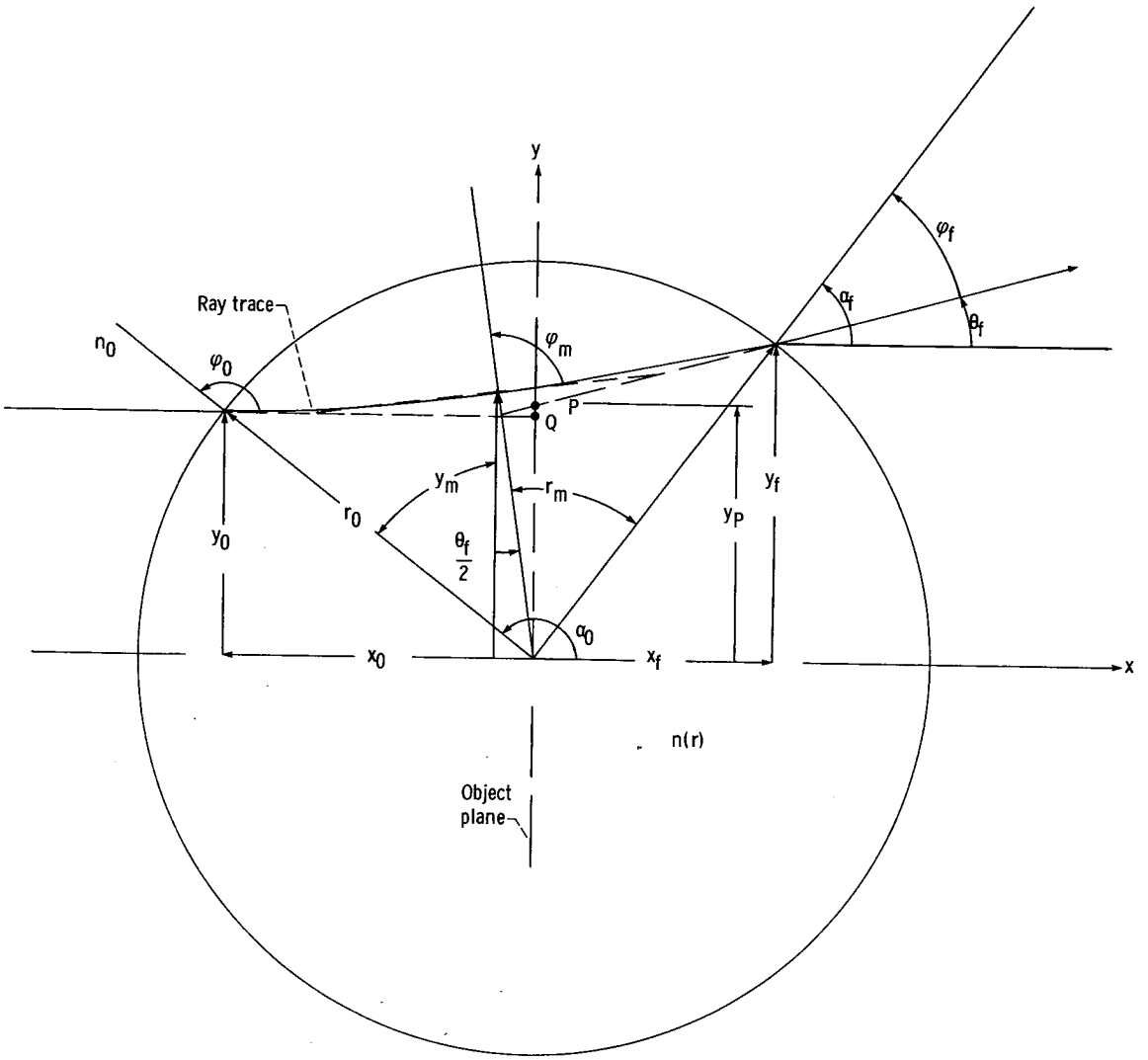

Figure 7. - Ray trace in medium with spherical, or axial, symmetry.

$$\frac{n_m - n_0}{n_0} = \frac{\theta_f}{4 \tan \alpha_0} \tag{4}$$

where α_0 is the initial angle formed by the radius r and a light ray at the value r_0 initially intercepted by the associated ray trace.

To evaluate $(n_m - n_0)/n_0$, note that

$$\theta_f = \tan^{-1}\left(\frac{d}{f}\right) \tag{5}$$

by virtue of equation (1). Also from figure 7 and equation (3)

$$\sin \alpha_0 = \frac{y_0}{r_0} = \frac{y_P}{r_0} \tag{6}$$

Thus, only f, d, y_P, and r_0 need be determined. The decollimator focal length f is readily measured. From the recorded rainbow schlieren transparency the color can be noted as a function of the ordinate y_P measured perpendicular to the axis of symmetry in the image plane. (Note that y_P is given by the measured ordinate value divided by the magnification of the image.) The deflection d is determined by measuring the radius at which the specified color occurs on the rainbow filter. Finally, the radius r_0 is given by the maximum value of y_P for which a rainbow color is observed on the transparency. After f, d, y_P, and r_0 have been evaluated $(n_m - n_0)/n_0$ can be calculated.

The rainbow schlieren method and evaluation equations are very much simpler than the corresponding interferometric method (refs. 8 to 10). However, this advantage may be countered by the increased detection threshold and lesser accuracy of the rainbow schlieren method. This remains to be determined.

By using the preceding equations the relative refractive index distribution was calculated from measurements on the rainbow schlieren transparency used to obtain figure 5(a). The results shown in figure 8 appear reasonable with regard to magnitude and distribution by comparison with graphs and data in references 11 and 12. For example, the maximum evaluated value of $(n_m - n_0)/n_0$ is of the order 10^{-4}, so that the corresponding temperature is of the order 10^3 K (ref. 11). This temperature is probably not unreasonably low considering that the fuel-air mixture was lean. The temperature distribution is qualitatively similar to those shown in reference 12.

Along the cone (the triangular region) of the thermal field in figure 5(a) the refractive index distribution presently cannot be determined because the preceding theory does not cover the case of the two-stage (combustion region, where $n = n(r)$, and cone, where n = constant) distribution observed in figure 5(a). Moreover, the true color of the distribution is obscured by intense diffraction fringes. Downstream of the cone the central portion of the temperature field cannot be determined because of insufficient refraction, which causes a broad axial region to appear uncolored. Nevertheless, it is evident from the numerical results that the absolute value of the refractive index difference $n_m - n_0$ declines toward the axis. Moreover, the maximum difference is not associated with the maximum deflection, that is, with the color red, because of the variation of ray-trace lengths through the field $n(r)$ as a function of the initial value y_0 for each trace. Since the refraction is weak across the entire axial region, the refractive index gradient must also be weak because the thickness of the inhomogeneity is relatively constant there. Hence the absolute refractive index difference in the axial region is probably not much less than that near the innermost evaluated points. The expected central distribution 10 nozzle-exit diameters downstream of the exit is indicated by the dashed portion of the distribution.

Note that the cited difficulties regarding evaluation of the core and axial region would not exist in studies of axial flows over axially symmetric bodies. Hence a more complete evaluation of these flows should be possible.

Hot Plate (Items (5) and (6))

Figures 9 and 10 show the refraction field above a hot plate consisting of an electrically heated, high-resistance coil. These schlieren photographs were obtained by using a rainbow filter 2.56 mm in diameter with a clear center 0.37 mm in diameter. Figure 9 shows the edge of the hot plate. The strong temperature gradient near the edge of the thermal field is evident. Near the coil edge the

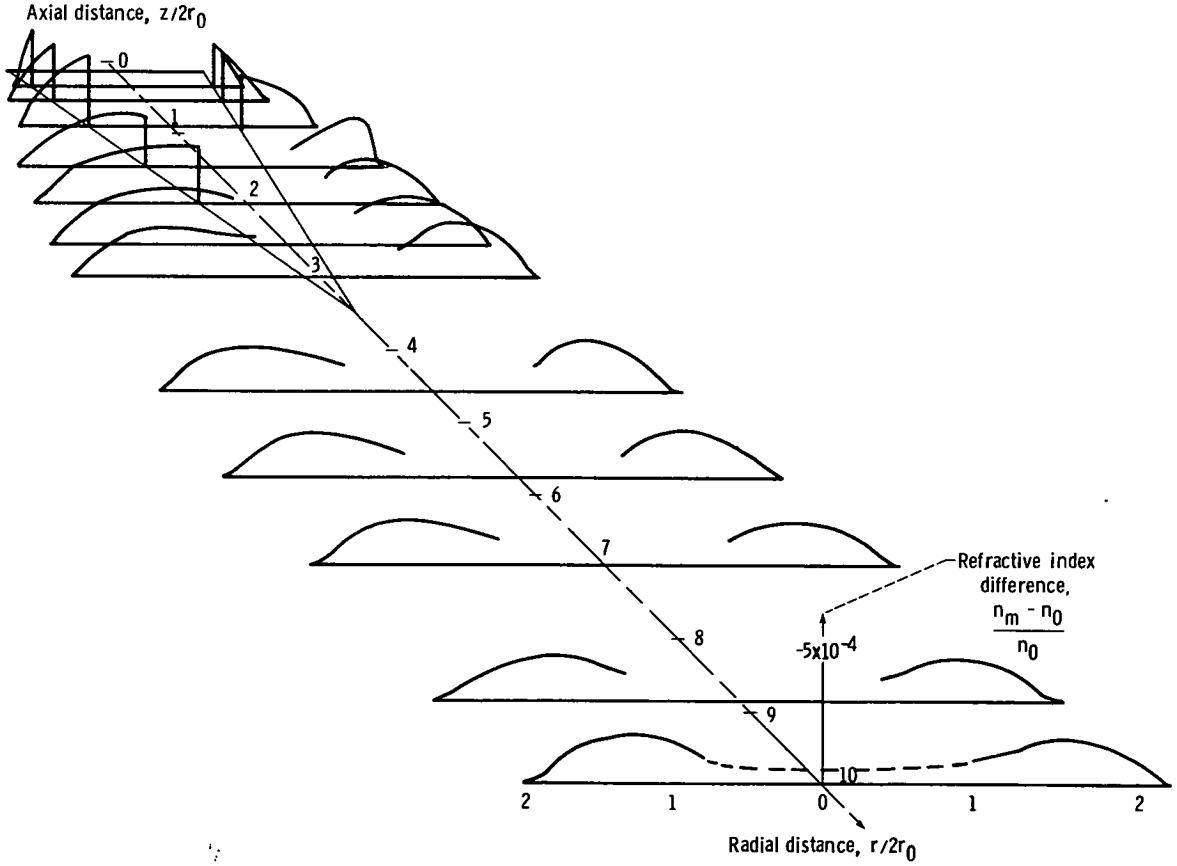

Figure 8. - Relative refractive index change above acetylene flame. Nozzle tilt, approximately 3.7° from vertical.

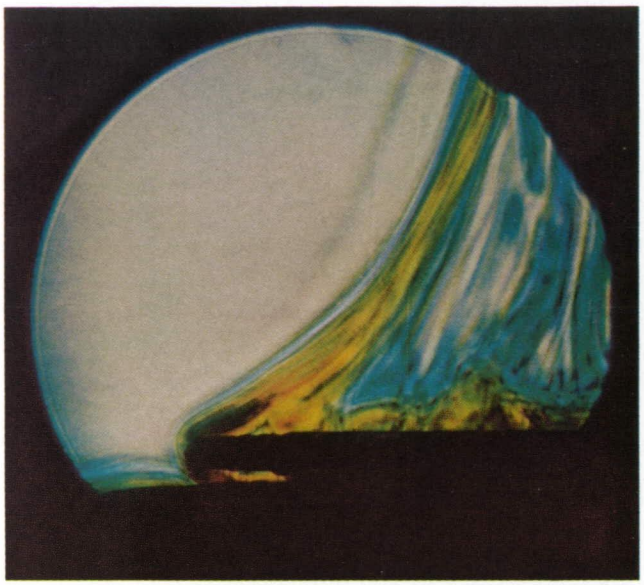

Figure 9. - Rainbow schlieren photograph of light refraction field above edge of hot plate.

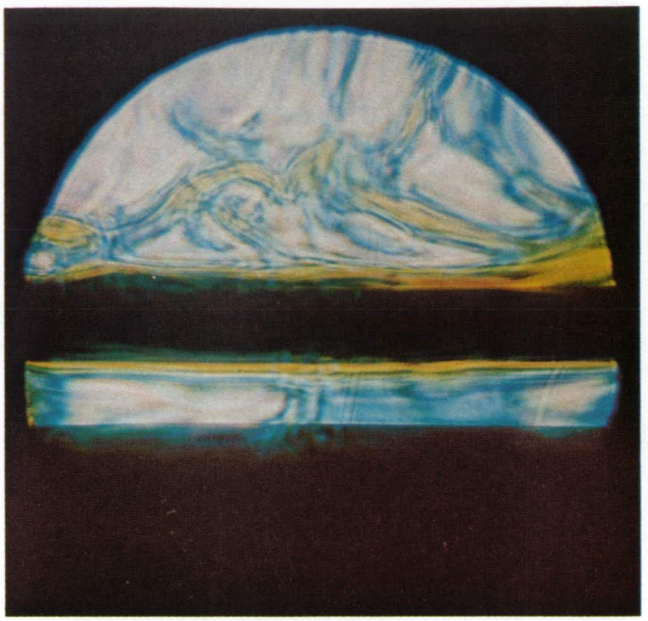

Figure 10. - Rainbow schlieren photograph of light refraction field induced by thick aluminum plate suspended above hot plate.

gradient is so large that the deflection of the light due to refraction exceeds the range of the rainbow filter. Hence the field appears black. The contraction of the refraction field as a function of distance above the plate is apparent from the shape of the thermal boundary. Significant local variations of the refraction field are also evident.

Figure 10 shows the refraction field near a thick (0.95 cm), square (15 cm by 15 cm) aluminum plate supported at two edges 1.3 cm above the hot plate. The photograph is for "steady state" conditions, that is, for a plate temperature independent of time. However, the thermal field is clearly unsteady. Beneath the thick plate the region of nonuniform temperature is quite thin. Most of the heat from the hot plate escapes from the open ends and sides between the plates. Above the thick plate the thermal boundary layer is thicker.

Color videotapes of dynamic events occurring during the time history of the heating process showed the complexity of the flow fields that arose at various stages of the process. For example, in the case of the aluminum plate suspended above the hot plate, weak temperature gradients appeared between the plates as heating commenced. These gradients did not increase in magnitude as heating progressed because the heat was convected from between the plates. However, as the aluminum plate warmed, a thin, thermal boundary layer formed beneath it. Then a similar boundary layer developed above the aluminum plate as the upper surface of this plate warmed. The upper layer became significantly thicker than the lower layer, and dynamic processes became much more evident in the region above the aluminum plate. In particular, the upper boundary layer fluctuated in thickness as thermal waves propagated across the plate surface. This occurred although the plate was horizontal in a presumably quiescent atmosphere. Moreover vortices were frequently observed arising from the plate surface. Finally volumes of overheated air were often cast off from the boundary layer and rose in the thermal chimney, appearing much like solar flares. The fields observed by using the rainbow schlieren were clearly far more detailed than those observed by using the black-and-white schlieren.

Glycerine-Water Mixture (Item (7))

A few ounces of glycerine were poured into a partially filled tank of water. The 14.9-cm-diameter cylindrical tank was 15.55 cm long and was bounded by 2.54-cm-thick, schlieren-quality, glass windows. The glycerine-water mixture was thoroughly stirred with a rod and then allowed to settle. Rainbow schlieren transparencies were recorded every few seconds at various stages of the settling process, and color videotapes were made of the entire process. The same rainbow filter was used as in the hot-plate tests (items (5) and (6)).

Immediately after being stirred the mixture appeared to have a fine filamentary, turbulent structure, essentially reddish orange in color. Increasing refraction toward the bottom of the tank implied settling of the glycerine. Within several seconds the turbulent structure slowly enlarged, and the color progressed through the spectrum to a mixture of green and blue with a red layer forming above a black layer at the bottom of the tank. This layered structure, shown in figure 11, persisted, even after 15 hr. It is noteworthy that, when the layered fluid was restirred, the colored, turbulent structure reappeared, but then faded away. Layering did not reappear. The fluid became clear. Apparently the

Figure 11. - Rainbow schlieren photograph of glycerine setting in water.

glycerine and water were now mixed completely on a molecular scale.

The color of the stirred fluid may provide a new and simple method for quantitatively estimating some characteristics of turbulence, since the color corresponds to a mean refraction that is related to mean characteristics of the turbulence (ref. 7). In the following paragraph equations are presented for evaluating refractive index fluctuations in homogeneous, isotropic turbulence.

Assume that the refractive index n of a fluid is given by

$$n = \bar{n} + \mu(x,y,z) \tag{7}$$

where $\bar{n}$ is the spatial mean value of refractive index along a ray trace, $\mu(x,y,z)$ is the refractive index perturbation, and $\mu << \bar{n} =$ constant. (The introduction of $\bar{n}$ herein in place of unity in ref. 7 is necessary for a fluid other than a gas.) It is shown in reference 7 that, for those conditions in which ray optics is valid and $D\sigma << 1$, the root-mean-square lateral deflection d_{rms} of a light-ray trace through homogeneous, isotropic turbulence is given by

$$d_{rms} = \frac{2}{\sqrt{3}} D^{1/2} \sigma^{3/2} \tag{8}$$

and the mean-square deflection angle θ_{ms} by

$$\theta_{ms} = 4D\sigma \tag{9}$$

where

$$D = \frac{\sqrt{\pi}\,\mu_{ms}}{\bar{n}^2 a} \tag{10}$$

is a "ray diffusion" coefficient, σ is the length of the ray trace, and a is the scale of the inhomogeneity. Since $D\sigma << 1$, it follows that $d_{ms}/\sigma << 1$, so that $\sigma \approx L$, where L is the test-section span containing the turbulence.

For small angles θ, the observed color is related to θ_{rms} by the formula

$$\theta_{rms} = \frac{d_{rms}}{f} \tag{11}$$

where, as before, d is the light-ray deflection at the rainbow filter, as indicated by the observed overall color of the turbulence, and f is the focal length of the decollimator. It follows from the preceding equations that the relative, root-mean-square, refractive index perturbation is then given by

$$\frac{\mu_{rms}}{\bar{n}} = \left(\frac{a}{4\sqrt{\pi}L}\right)^{1/2} \theta_{rms} \tag{12}$$

where a can be estimated as being one-half the eddy diameter indicated by rings of uniform color in the image. The refractive index perturbations are uniquely associated with other quantities, such as density (ref. 13).

The relative refractive index perturbations were evaluated from three transparencies recorded several seconds apart after the stirring process. An example is shown in figure 12. The overall color of selected regions of each transparency was observed and expressed in terms of d_{rms} on the basis of known dimensions of the rainbow filter. A characteristic turbulence scale ma ($m =$ magnification) in the horizontal direction was estimated from several measurements of horizontal diameters of eddies, as indicated by rings of uniform color. A magnified portion of figure 12 is shown in figure 13 to illustrate eddies. The length measurements were corrected for magnification to obtain the actual scale a. The calculated values were used to estimate the relative, root-mean-square, refractive index perturbation $\mu_{rms}/\bar{n}$. The data and results are listed in table I. The average eddy sizes ranged from approximately 1.3 to 3.4 mm, whereas $\mu_{rms}/\bar{n}$ ranged from approximately 2×10^{-5} to 7×10^{-5}. The magnitude of these perturbations increased as a function of time because the eddy sizes increased. The magnitude of perturbations increased as a function of depth because the root-mean-square refraction increased as a function of depth.

It is suggested as a consequence of the preceding results that the rainbow schlieren may be useful for evaluating turbulence and for determining when fluids have become mixed on a molecular scale.

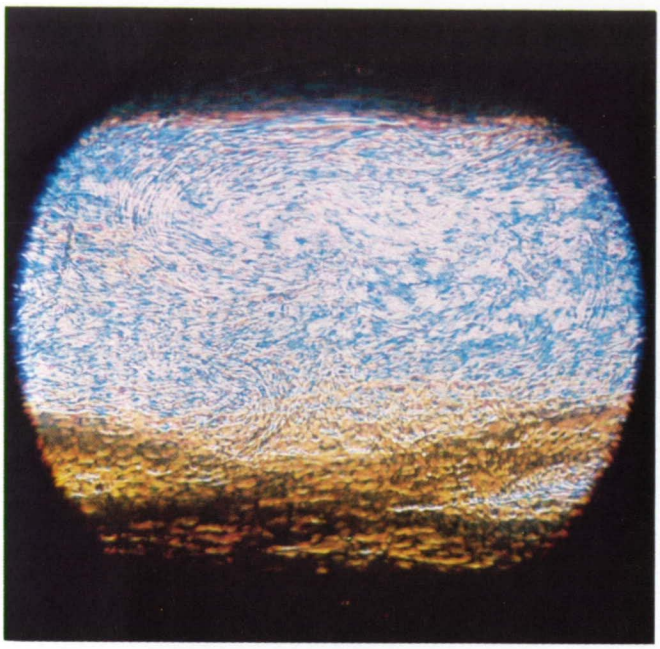

Figure 12. - Rainbow schlieren photograph of glycerine-water mixture shortly after stirring.

Plastic Sheet (Item (8))

Figure 14 is a rainbow schlieren photograph of a thin, transparent plastic sheet used in packaging gifts. The same rainbow filter was used as in recording the refraction field of the torch (item (1)). The nonuniformity of the refractive index or the thickness of the plastic is evident from the color variations. A granular effect is noticeable. Possibly the rainbow schlieren could be used to inspect or control the quality of transparent sheet materials, especially with regard to thickness and homogeneity.

Diffraction and Other Effects

The diffraction effects observed in schlieren photographs must be caused by some out-of-focus object along the light path. Since the camera is focused on objects in the test section, the obvious source of diffraction must be other objects interposed in the light path, specifically the knife edge in the black-and-white schlieren apparatus and the rainbow filter in the color schlieren apparatus.

A series of tests were performed to isolate the cause of the diffraction. The test-section-image plane and the light-source-image plane were carefully observed without and with the field half blocked by a straight-edge opaque plane inserted in the test-section-object plane. First, nothing, then a knife edge, a monochrome transparency, and a rainbow filter were successively introduced at the light-source-image plane. From these tests it was evident that the plane half-blocking the test section produced a diffracted, slit-like irradiance distribution at the light-source-image plane and that the rainbow filter then acted, by virtue of its nonuniform chromatic filtering characteristic, to produce an unsharp image of the edge. This effect can be observed in the nozzle image in figure 5(a).

The observed diffraction fringes are a more complicated phenomenon. In figure 5(a), in order of

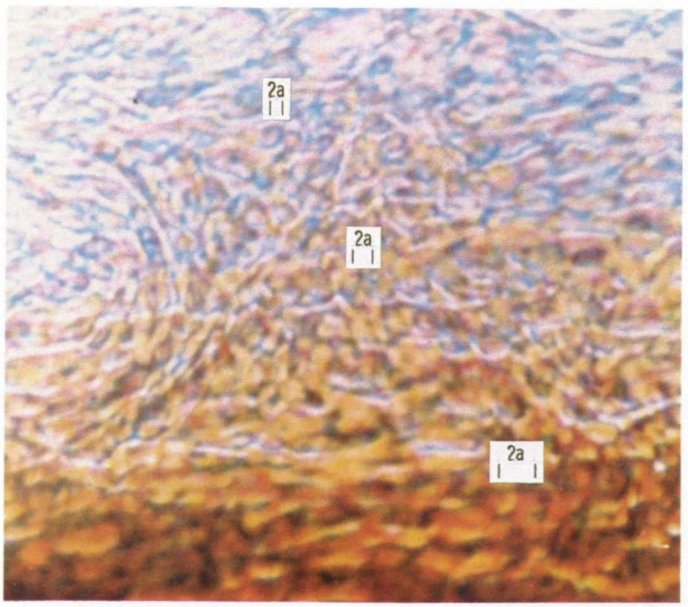

Figure 13. - Rainbow schlieren photograph of magnified region of glycerine-water mixture in figure 12.

TABLE I. – TURBULENCE DATA FOR GLYCERINE-WATER MIXTURE

Transparency	Average color	Average deflection, d_{rms}, mm	Average refraction angle, i_{rms}, rad	Turbulence scale, a, mm	Relative refractive index perturbation, d_{rms}/a
1	Yellow	0.781	1.24×10^{-3}	0.67	3.05×10^{-5}
2	Yellow	.781	1.24×10^{-3}	.90	3.55×10^{-5}
3	Blue	.306	4.86×10^{-4}	1.68	1.90×10^{-5}
	Yellow	.781	1.24×10^{-3}	1.19	4.07×10^{-5}
	Red	1.097	1.74×10^{-3}	1.70	6.84×10^{-5}

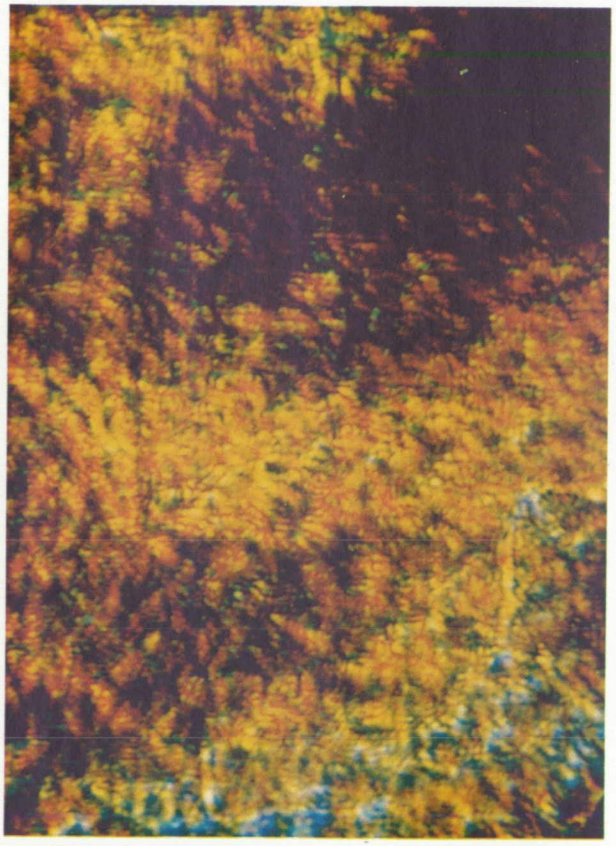

Figure 14. - Rainbow schlieren photograph of plastic sheet.

decreasing intensity these fringes are observed adjacent to

(1) Discontinuous refractive index boundaries associated with diffraction as well as refraction (the central cone)

(2) Color boundaries associated with weak refraction (the outer edge of the colored thermal boundary as well as the inner edge of the colored boundary)

(3) Solid boundaries associated with diffraction (the nozzle)

Since the camera was focused on the midspan plane of the test object (the flame), diffracted light from this plane was focused at the image plane.

Diffraction fringes then do not appear in the image. However, if a rainbow filter is introduced at the light-source image, any light that has been deviated from its ideal path by refraction or diffraction in the test section will traverse colored areas of the filter, including the boundary between the clear and blue sections of the filter. This filter boundary, which acts as a diffracting edge, will introduce additional diffraction that will not be focused at the image plane. Hence diffraction fringes should then appear in the image, as observed.

Additional, dark, diffraction fringes appear adjacent to the red, maximum-refraction region in figure 5(a). These fringes can be explained in the same way as the other fringes, except that the diffracting edge is the boundary between the red annulus of the filter and the black surround. This implies that the filter diameter was too small to contain all refracted light.

No attempt was made to minimize diffraction effects because their cause was not isolated until after the experiments illustrating applications of the rainbow schlieren were completed. However, diffraction minimization might be possible by defocusing the clear-blue boundary (defocusing plane A in fig. 3) when making the exposure for the clear center in the final filter.

In those tests in which the refractive index gradients developed slowly in time (items (5) and (6)) the first indication of color effects was the appearance of weak distributions of the nonspectral colors cyan and magenta in the disturbance field. These colors were soon dominated by the much more vivid spectral colors of the filter. Some evidence of the weak nonspectral colors still existed, however, as can be seen in the upper left of figure 10. In those tests in which the refraction was too weak (items (9) to (15), not shown) to display the refraction colors, the colors cyan and magenta nevertheless appeared. The cause of the nonspectral colors has not been determined.

In figure 10 an additional effect is evident that requires explanation. Specifically the plate surfaces do not appear straight but rather are wavy and obscure. Several effects might contribute to this phenomenon, namely geometrical distortion due to refraction, diffraction by the filter, diffraction by the edge of the plate nearest the

light source, and reflection from the plate surface. Since all surfaces were hotter than the adjacent gas and the plates were carefully alined, light would be refracted away from the plate surfaces, not into them. Hence reflection of light off plate surfaces is not a likely factor causing surface obscuration. Also, as can be seen from the region of the circular border and the upper surface of the hot plate, which appears straight, diffraction fringes tended to be localized or weak. Hence diffraction effects do not appear to be the dominant cause of obscuration. Rather, large refraction effects resulting from large changes in thermal gradients and from the large span (15.55 cm) of the upper plate may be the dominant feature.

With regard to refraction the camera was focused on the midspan plane of the plate. For a constant refractive index gradient the distortion of the object plane should vanish when focus is on the midspan plane (ref. 6). However, if the refractive index gradient is not constant, the residual distortion Δ (D in ref. 6), readily derivable to the next order of approximation from reference 6, is given by

$$\Delta = \pm \frac{1}{24} \left(\frac{dn}{dy} \right)_{y_0} \left(\frac{d^2n}{dy^2} \right)_{y_0} L^4 \tag{13}$$

where dn/dy is the refractive index gradient normal to the initial ordinate y_0 at which a light ray enters the test section and L is the test-section span. The amount by which the apparent locations of object points are shifted from their true locations is given by this equation. In figure 10 the appearance of fluid effects superimposed on what appears to be the plate's cross-section can be explained in terms of refraction as apparent-ray-trace crossing in which light associated with two or more points in the object plane appears to originate from the same point (ref. 6).

Conclusions

The rainbow schlieren has been shown to be a simple and useful instrument providing much greater detail regarding refractive index nonuniformities than does the ordinary black-and-white schlieren with a knife-edge cutoff. Moreover the rainbow schlieren is capable of providing quantitative information in many situations, including turbulence studies, in which the ordinary schlieren can yield quantitative results only with the greatest difficulty or not at all. The calculations required when using the rainbow schlieren are extremely simple.

Lewis Research Center
National Aeronautics and Space Administration
Cleveland, Ohio, February 2, 1983

Appendix A
Symbols

a scale of turbulent inhomogeneity
D "ray diffusion" coefficient (eq. (10))
d light-ray deflection at image of light source
f focal length of schlieren decollimator
K constant for individual ray trace (eq. (B1))
L test-section span
m magnification
n refractive index
n_0 ambient refractive index
r radius from center of field symmetry to ray trace
x Cartesian coordinate (abscissa) parallel to incident ray trace and with origin at center of field symmetry (fig. 7)
y,z Cartesian coordinate (ordinate) perpendicular to incident ray trace and with origin at center of field symmetry (fig. 7)
α angle between light-ray trace and x axis
Δ distortion (defined as $y_P - y_0$, eq. (B6))
θ angle of refraction
μ refractive index perturbation
σ length of ray trace in turbulent medium
φ angle between light-ray trace and radius r

Subscripts:

f final value in medium with refractive index $n(r)$
m value associated with closest approach of ray trace to center of symmetry of refractive index field $n(r)$
max maximum value achieved in an experiment
ms mean square
P refers to object point P
rms root mean square
0 initial value, at boundary where $n(r) \to n_0$

Superscript:

$\bar{}$ spatial mean value along ray trace

Appendix B
Refractive-Index-Field Evaluation Equations for a Medium with Spherical Symmetry

The path of a light ray through a medium with spherical symmetry is given by (ref. 5, p. 122)

$$nr \sin \varphi = K = \text{constant} \tag{B1}$$

where $n = n(r)$ is the refractive index, a function of radius r; r is the radius of a ray trace from the center of symmetry; and φ is the angle formed by the ray and the radius r.

Assume that, at some radius value r_0, shown in figure 7, the continuous refractive index distribution $n(r)$ attains the uniform, ambient value n_0. At this initial boundary at which the ray trace first encounters $n = n(r)$, equation (B1) satisfies

$$n_0 r_0 \sin \varphi_0 = K$$

Assume that the ray is initially parallel to the x axis of an x,y,z-coordinate system. Then initially

$$\varphi_0 = \alpha_0$$

and

$$y_0 = r_0 \sin \varphi_0 = \frac{K}{n_0} = r_0 \sin \alpha_0 \tag{B2}$$

where α is the angle formed by the radius r and the x axis and y is the ordinate value of the ray.

At the minimum radius r_m attained by the ray trace, $\sin \varphi_m = 1$. Hence

$$r_m = \frac{K}{n_m} \tag{B3}$$

where n_m is the refractive index at radius r_m. By combining equations (B2) and (B3),

$$\frac{n_m}{n_0} = \frac{y_0}{r_m} \tag{B4}$$

where, without loss of generality, $y_0 > 0$. Alternatively

$$\frac{n_m - n_0}{n_0} = \frac{y_0 - r_m}{r_m} \tag{B5}$$

which determines the relative refractive index difference at r_m if y_0 and r_m can be determined. The ratio $(n_m - n_0)/n_0$ defined at radius r_m is determined by observations made at the apparent object point P at ordinate value y_P in the object plane, that is, at the backward extension to the object plane of the ray emerging from the nonuniform distribution $n = n(r)$, as shown in figure 7. The initial ordinate value y_0 of the real object point corresponds to point Q at the forward extension to the object plane of the ray initially incident on $n = n(r)$.

To determine the values of r_m and y_0 relative to the ordinate value y_P of the apparent object point P, consider two distances:

(1) The difference $y_P - r_m$ between the ordinate value of the apparent object point P and the minimum radial value of the ray trace

(2) The distortion Δ defined by

$$\Delta \equiv y_P - y_0 \tag{B6}$$

which specifies the ordinate displacement of the apparent object point due to refraction

For ease of evaluation

$$y_P - r_m = y_P - y_f + y_f - r_m \tag{B7}$$

Assume that the product $n(r)r$ is monotonic. This should generally be valid for continuous refractive index changes in gases. Then ray traces will be symmetric about corresponding radii r_m (ref. 4, p. 167). Because of this symmetry

$$\alpha_f = \varphi_f + \theta_f = \pi - \alpha_0 + \theta_f$$

so that

$$y_f = r_\theta \sin \alpha_f = r_0 \sin(\alpha_0 - \theta_f) = y_0 \cos \theta_f - x_0 \sin \theta_f \tag{B8}$$

where y_0 is given by equation (B2), and

$$x_0 = r_0 \cos \alpha_0 \tag{B9}$$

In a similar manner the last two terms in equation (B7) yield

$$y_P - y_f = -x_f \tan \theta_f = r_0 \cos(\alpha_0 - \theta_f) \tan \theta_f$$
$$= (x_0 \cos \theta_f + y_0 \sin \theta_f) \tan \theta_f \tag{B10}$$

Since r_m is a function of $n(r)$, which is not known explicitly, r_m must be approximated. Because of symmetry the refraction angle is $\theta_f/2$ at r_m. Hence,

$$r_m = \frac{y_m}{\cos(\theta_f/2)} \tag{B11}$$

From figure 7,

$$\begin{aligned} y_0 < y_m < y_0 + \frac{y_f - y_0}{2} \quad &\text{if } y_f > y_0 \text{ (i.e., if } n_0 > n_m) \\ y_0 > y_m > y_0 + \frac{y_f - y_0}{2} \quad &\text{if } y_f < y_0 \text{ (i.e., if } n_0 < n_m) \end{aligned} \tag{B12}$$

where

$$y_0 + \frac{y_f - y_0}{2} = \frac{1}{2} y_0 (1 + \cos\theta_f) - \frac{1}{2} x_0 \sin\theta_f$$

by virtue of equation (B8). For $\alpha_0 \to \pi$ this expression approaches y_0 because $\theta_f \to 0$. For $\alpha_0 \to \pi/2$ it approaches y_0 because $x_0 \to 0$ and $\theta_f \to 0$. In the intermediate range $\pi/2 < \alpha_0 < \pi$, assume that y_m is intermediate between the potential limits indicated by inequality (B12). Then,

$$y_m = y_0 + \frac{y_f - y_0}{4} = \frac{1}{4} y_0 (3 + \cos\theta_f) - \frac{1}{4} x_0 \sin\theta_f$$

so that equation (B11) becomes

$$r_m = \frac{1}{4} \left(\cos\frac{\theta_f}{2}\right)^{-1} [y_0 (3 + \cos\theta_f) - x_0 \sin\theta_f] \tag{B13}$$

Therefore, by virtue of equations (B7), (B8), (B10), and (B13),

$$\begin{aligned} y_P - r_m = \frac{1}{4} x_0 \sin\theta_f \left(\cos\frac{\theta_f}{2}\right)^{-1} \\ - y_0 \left[\frac{1}{4} (3 + \cos\theta_f) \left(\cos\frac{\theta_f}{2}\right)^{-1} \right. \\ \left. - \cos\theta_f - \sin\theta_f \tan\theta_f \right] \end{aligned} \tag{B14}$$

By expanding $(\cos\theta_f/2)^{-1}$ as

$$\left(\cos\frac{\theta_f}{2}\right)^{-1} = 1 + \frac{\theta_f^2}{8} - + \ldots \tag{B15}$$

it follows that, for small θ_f,

$$y_P - r_m = \frac{x_0 \theta_f}{4} \tag{B16}$$

so that

$$|y_P - r_m| < \left| \frac{r_0 \theta_{\max}}{4} \right| \tag{2}$$

determines the upper limit on the difference, where $\theta_{\max}$ is the maximum value of θ_f.

For ease of evaluation the distortion Δ can be expressed as

$$\Delta = y_P - y_f + y_f - y_0 \tag{B17}$$

which, by virtue of equations (B8) and (B10), becomes

$$\Delta = y_0 \left(\frac{1 - \cos\theta_f}{\cos\theta_f} \right)$$

For small θ_f,

$$\Delta = \frac{y_0 \theta_f^2}{2} \tag{B18}$$

which possesses the upper limit

$$\Delta < \frac{r_0 \theta_f^2}{2} \tag{3}$$

The refractive index ratio $(n_m - n_0)/n_0$ can now be written for small θ_f as

$$\frac{n_m - n_0}{n_0} = \frac{\theta_f/4}{\tan\alpha_0 - (\theta_f/4)} \tag{B19}$$

by using equations (B5), (B13), and (B15). In the special case $\alpha_0 \neq \pi$,

$$\frac{n_m - n_0}{n_0} = \frac{\theta_f}{4 \tan\alpha_0} \tag{4}$$

which vanishes as $\alpha_0 \to \pi/2$.

References

1. Schardin, H.: Schlieren Methods and Their Applications. NASA TT F-12731, 1970. (Translation from Ergeb. Exakten Naturewiss., vol. 20, 1942, pp. 303–433.)
2. Merzkirch, W.: Flow Visualization. Academic Press, 1974, pp. 86–102.
3. Settles, G. S.: Color Schlieren Optics—A Review of Techniques and Applications. International Symposium on Flow Visualization, Ruhr-Universitaet, Bochum, 1981, pp. 187–197.
4. Luneberg, R. K.: Mathematical Theory of Optics. Univ. California Press, 1964.
5. Born, M.; and Wolf, E.: Principles of Optics. Pergamon Press, 1959.
6. Howes, W. L.; and Buchele, D. R.: Optical Interferometry of Inhomogeneous Gases. J. Opt. Soc. Am., vol. 56, no. 11, Nov. 1966, pp. 1517–1528.
7. Chernov, L. A.: Wave Propagation in a Random Medium. Dover Publications, Inc., 1967, Chapter 2.
8. Schardin, H.: Theory and Applications of the Mach-Zehnder Interference-Refractometer. Defense Research Lab., Univ. Texas, Rept. T-3, 1946. (Translation from Z. Tech. Phys., vol. 12, 1931, p. 436 ff.)
9. Bradley, J. W.: Density Determination from Axisymmetric Interferograms. AIAA Journ., vol. 6, no. 6, 1968, pp. 1190–1192.
10. Vest, C. M.: Interferometry of Strongly Refracting Axisymmetric Phase Objects. Appl. Opt., vol. 14, no. 7, July 1975, pp. 1601–1606.
11. Weinberg, F. J.: Optics of Flames. Butterworths, 1963, p. 29.
12. Lewis, B.; and von Elbe, G.: Combustion, Flames and Explosions of Gases. Second Ed. Academic Press, 1961, pp. 280f, 706.
13. von Hippel, A.: Dielectrics. Handbook of Physics. (E. U. Condon, and H. Odishaw, eds., McGraw-Hill Book Co., Inc., 1958, Part 4, Chapter 7, p. 113.

1. Report No. NASA TP-2166	2. Government Accession No.	3. Recipient's Catalog No.
4. Title and Subtitle RAINBOW SCHLIEREN		5. Report Date May 1983
		6. Performing Organization Code 505-32-82
7. Author(s) Walton L. Howes		8. Performing Organization Report No. E-1173
9. Performing Organization Name and Address National Aeronautics and Space Administration Lewis Research Center Cleveland, Ohio 44135		10. Work Unit No.
		11. Contract or Grant No.
12. Sponsoring Agency Name and Address National Aeronautics and Space Administration Washington, D. C. 20546		13. Type of Report and Period Covered Technical Paper
		14. Sponsoring Agency Code

15. Supplementary Notes

16. Abstract

The rainbow schlieren is a new apparatus in which the usual schlieren knife-edge cutoff is replaced by a radial rainbow filter with a transparent center and an opaque surround. With this apparatus most refractive index nonuniformities in the test section appear varicolored whereas uniformities appear white. The rainbow schlieren is simple, easy to use, and relatively inexpensive and gives much greater detail regarding nonuniformities than does the ordinary schlieren. Moreover, the rainbow schlieren permits quantitative evaluation of certain refractive index distributions, including those involving turbulence, by simple calculations.

17. Key Words (Suggested by Author(s))	18. Distribution Statement
Schlieren; Color; Light; Optics; Refraction; Fluid flow; Deformation; Turbulence	Unclassified - unlimited STAR Category 35

19. Security Classif. (of this report)	20. Security Classif. (of this page)	21. No. of Pages	22. Price*
Unclassified	Unclassified	20	A02

* For sale by the National Technical Information Service, Springfield, Virginia 22161

☆ U.S. GOVERNMENT PRINTING OFFICE: 1983—661-154

ERRATA

NASA Technical Paper 2166

RAINBOW SCHLIEREN

Walton L. Howes
May 1983

Page 2, figure 1: The rightmost vertical line should be labeled "Test-section image plane, I."

Pages 7 and 17, equation (3): The symbol θ_f should be θ_{max}.

Page 9, left column, line 11: The word "lean" should be replaced with the word "rich."

Page 11, figure 11: The legend should read "Rainbow schlieren photograph of glycerine settling in water."

Page 11, left column, equation (8) and second line above it: The symbol d_{rms} should be replaced by δ_{rms}.

Page 11, right column, line 4: The symbol d_{rms} should be replaced by δ_{rms}.

Page 12, figure 13: Labels denoting 2a are misplaced.

Page 13, table I, third column: The symbol should be δ_{rms}.

Page 13, table I, fourth column: The symbol should be θ_{rms}.

Page 13, table I, sixth column: The symbols should be $\mu_{rms}/\overline{n}$.